JOURNAL OF CATALYSIS 110, 298–309 (1988)

Carbon Monoxide and Propene Oxidation by Iron Oxides for Auto-Emission Control

J. S. WALKER,[1] G. I. STRAGUZZI, W. H. MANOGUE,[2] AND G. C. A. SCHUIT

Center for Catalytic Science and Technology, Department of Chemical Engineering, University of Delaware, Newark, Delaware 19716

Received June 22, 1987; Revised October 8, 1987

Activities of iron-based materials for the simultaneous total oxidation of CO and C_3H_6 were measured under conditions that were typical of automotive operation: space velocity of 35,000 h^{-1}; temperatures between 373 and 873 K; atmospheric pressure; feed composition of 2.5% CO, 1.7% O_2, 0.5% H_2, 0.05% C_3H_6, and, optionally, 0.004% SO_2 in He. In the absence of SO_2, activity decreased in the order $Fe_2O_3/Al_2O_3 > Fe_2O_3/TiO_2 \sim Fe_2O_3 \gg FeSbO_4 > FePO_4 > Fe_2(MoO_4)_3$. CO and C_3H_6 removal followed apparent first-order kinetics and the data showed a compensation law effect. Oxidation was inhibited when SO_2 was present; temperatures for CO conversion over Fe_2O_3 were raised about 160 K, while the comparable rise for C_3H_6 oxidation was about 80 K. Inhibition was less with Fe_2O_3 on 35 m^2/g TiO_2 than with Fe_2O_3 on 350 m^2/g Al_2O_3 or with unsupported 5 m^2/g Fe_2O_3. Both $FeSbO_4$ and $FePO_4$ showed good activity for the conversion of C_3H_6, but not of CO, when SO_2 was absent. Material balances indicate that the partial oxidation product acrolein inhibits CO oxidation over these binary "selective oxidation" catalysts. Collectively, the data suggest that an inhibitor is created by oxidation of a precursor and its oxidation can be inhibited by the product of another feed component through control of the size of reactive ensembles on the catalyst surface.

INTRODUCTION

The main difficulty in the application of automotive exhaust gases catalysts prepared from base metals is their sensitivity to poisoning by trace amounts of SO_2, always present in the exhaust gases. According to a number of investigators (*1–4*), the sulfur inhibition is due to the formation of a layer of sulfate on the surface of the catalyst; SO_2 apparently is catalytically oxidized to SO_3 that is subsequently adsorbed on the active surface. A good catalyst should therefore be selective in oxidizing CO and hydrocarbons to CO_2 and H_2O but not SO_2 to SO_3 (or should not form a stable sulfate (*5*)).

All catalysts discussed in this report have iron oxide as one of their components. Although not necessarily the most promising among the base metal oxides, they offered advantages with respect to the analysis of the interactions of various feed components during oxidation. Another reason in their selection was the availability of well-characterized binary Fe oxides, such as $FeSbO_4$, $FePO_4$, and $Fe_2(MoO_4)_3$, already known to be selective in the oxidation of olefins and methanol. Since the study was exploratory in nature, the feed composition was fixed at 2.5% CO + 1.7% O_2 + 0.5% H_2 + 500 ppm C_3H_6 and, optionally, 40 ppm SO_2 in helium. The space velocity was constant at 35,000 h^{-1} and the only kinetic parameter varied was the temperature.

PREPARATION AND CHARACTERIZATION OF THE CATALYSTS

Fe_2O_3—100 mesh. Used from the bottle (MCB), Fe_2O_3 had a surface area of 5.3 m^2/g. Traces of P and S impurities were detected by X-ray fluorescence (XFR), and X-ray diffraction (XRD) indicated the sam-

[1] Present address: Air Products and Chemicals, Inc., Allentown, PA 18105.

[2] To whom correspondence should be addressed at E. I. du Pont de Nemours and Company, Experimental Station, B262, Wilmington, DE 19898.

0021-9517/88 $3.00

ple to be pure crystalline hematite phase (*6*). Table 1 shows the surface composition as given by XPS. XPS samples were cooled down to room temperature under reactant gases and purged with helium. Samples were mounted by spreading fine powder on vacuum-compatible adhesive tape. No significance is attached to the carbon data, since fresh and used samples generally showed similar amounts of carbon.)

Supported Fe_2O_3. TiO_2 (CS-200 spheres, Sakai Chemicals, pore volume 0.39 cc/g, crushed to 30–48 mesh) and Al_2O_3 (Alcoa-activated T255, γ-Al_2O_3) were impregnated by incipient wetness with a solution of iron nitrate (*8*). Several impregnations were needed to attain the desired Fe concentration. The samples were further calcined at 770 K. The surface area of Fe_2O_3/TiO_2 was 23.8 m^2/g; XRD showed a mixture of rutile and Fe_2O_3 which was unchanged after reaction. The Fe_2O_3/Al_2O_3 area was 269 m^2/g; XRD showed difficult-to-resolve Fe_2O_3 that changed to maghemite (*7*) after reaction.

$FeSbO_4$. This catalyst was prepared by precipitation with NH_4OH, adding an $Fe(NO_3)_3$ (Fisher) solution to a slurry of Sb_2O_3 (Chemetron) in diluted acetic acid (*9*). The catalyst was calcined in flowing air at 973 K. It had a surface area of 29.2 m^2/g; XRD showed a tetragonal structure (*6*) with traces of unreacted Sb_2O_3. The surface composition, as given by XPS, is presented in Table 2.

$FePO_4$. This catalyst was prepared by titrating a stoichiometric solution of ferric nitrate in phosphoric acid with NH_4OH to a pH of 6–8, while continuously stirring with mild heating. Part of the dried and filtered precipitate was calcined in flowing air at 770 K, and part at 970 K. The XRD pattern for the 770 K calcined sample indicated that the solid was largely amorphous, while the pattern for the sample calcined at 970 K matched that of hexagonal $FePO_4$ (*6*). A +48 mesh sample of the amorphous catalyst was tested. It had a surface area of 99.4 m^2/g. Its surface composition is given in Table 3.

$Fe_2(MoO_4)_3$. Prepared by coprecipitation (*10*), $Fe_2(MoO_4)_3$ had a surface area of 2.4 m^2/g. XRF indicated traces of S and Ge as major impurities. The XRD pattern matched that of monoclinic iron molybdate with small amounts of MoO_3 (*6*). The surface composition had the largest variations between fresh and used, of all the catalysts tested (Table 4).

TABLE 2

Surface Composition of $FeSbO_4$ (at.%) by XPS

	Fe	Sb	C	S
Prerun	6.5	26.2	61.4	5.9
Postrun	4.9	24.3	48.5	22.4

MATERIALS, APPARATUS, AND EXPERIMENTAL TECHNIQUES

All gases used were research purity from Matheson Gas Products. C_3H_6 was purchased as a 3% mixture in helium; SO_2 as a 0.25% mixture. Figure 1 is a flowsheet of the single-pass reactor used to test the samples. The standard loading was 1 g of catalyst mixed with 5 g of SiC in a quartz tube inserted in an electric heater with an aluminum heat sink to minimize hot spots. The gas flow rate was 1000 cc/min and the pressure close to atmospheric. Although some runs were isothermal, most of the experi-

TABLE 1

Surface Composition of Fe_2O_3 (at.%) by XPS

	Fe	O	C	S
Prerun	30.3	56.6	13.1	—
Postrun	27.2	59.0	11.5	2.5

TABLE 3

Surface Composition of $FePO_4$ (at.%) by XPS

	Fe	P	O	C
Prerun	11.0	11.9	58.4	18.8
Postrun	11.5	12.9	50.0	26.1

TABLE 4

Surface Composition of $Fe_2(MoO_4)_3$ (at.%) by XPS

	Fe	Mo	O	C
Prerun	4.8	11.7	50.6	32.9
Postrun	10.5	4.5	49.6	35.1

ments were done in the temperature scanning mode, heating and cooling the reactor between 373 and 873 K at a controlled rate, while scanning the conversions of CO and propylene in the absence of SO_2. If the activities were within acceptable limits, the catalyst was tested with SO_2 added to observe how well it maintained its activity. Pt/Al_2O_3, currently a component in commercial automotive catalytic converters, was chosen as standard for judging new catalysts (Fig. 2). Reactor effluent was analyzed on stream by two calibrated thermal-conductivity gas chromatographs coupled with integrators. A 13× molecular sieve column was used to analyze CO and O_2, and a 2.4-m Poropak Q/R column was used for CO_2, water, and hydrocarbons. Column operation was isothermal to permit more frequent sampling; but as a result by-products, such as acrolein, were not determined. Estimates of propylene conversion to acrolein, and of hydrogen consumption, were calculated from material balances.

EXPERIMENTAL RESULTS

In Fig. 3, an example is presented of the type of data obtained by scanning the conversions of CO and C_3H_6 as a function of temperature in the absence or presence of SO_2; the catalyst used here was Fe_2O_3/TiO_2. Figure 4 shows the same data plotted according to Eq. (1),

$$\ln[-\ln(1 - x)] = \ln A' - E'/R * 1000/T_x, \quad (1)$$

where x is the fraction of C_3H_6 or CO converted at the temperature T_x; E' and $\ln A'$ are the (pseudo)-activation energy and logarithm of the preexponential constant of a

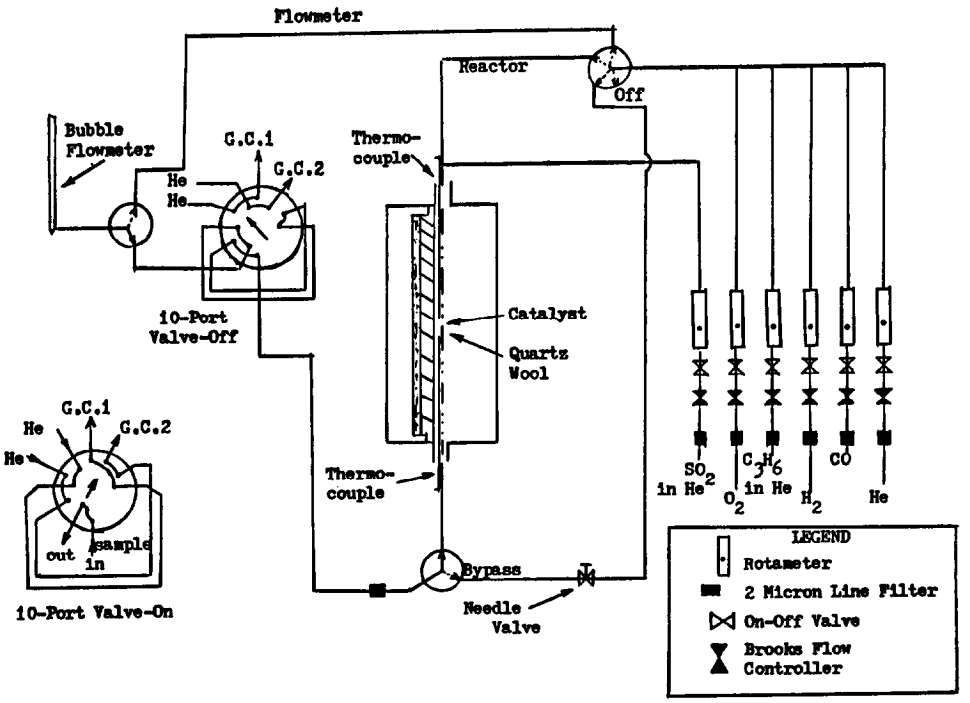

FIG. 1. Schematic diagram of gas manifold and reactor/bypass loops.

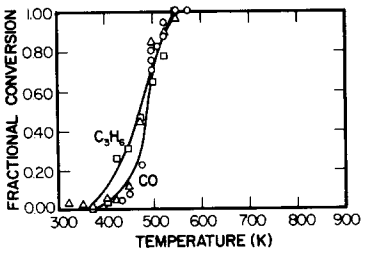

FIG. 2. Conversions of C_3H_6 and CO as a function of temperature in the absence of SO_2 over 0.5% Pt on γ-Al_2O_3 (1 g, $\frac{1}{8}$-in. × $\frac{1}{8}$-in. pellets mixed with 5 g 6–10 mesh acid-washed SiC). (□) C_3H_6 heating; (△) CO heating; (○) CO cooling.

first-order reaction that gave the best fit to the experimental data points. The results for the various catalysts are presented in Table 5, which also includes the degree of fit, n being the number of data points, and R, the correlation coefficient.

To obtain an estimate of the errors introduced by fitting with a first-order equation, similar calculations were done using half-order and zero-order functions. The results

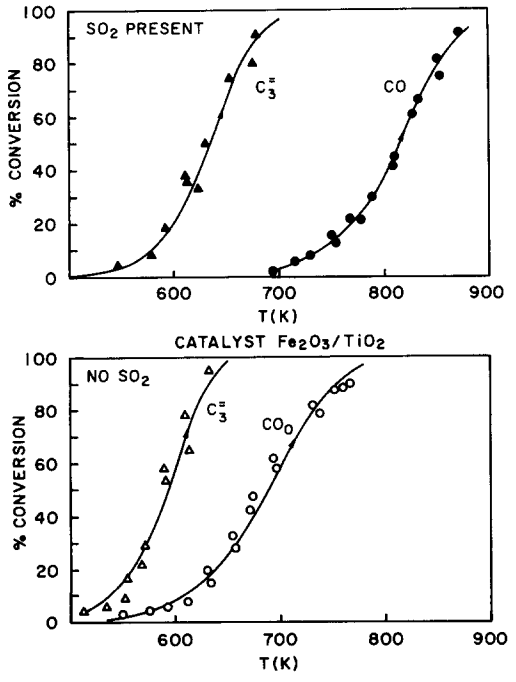

FIG. 3. Conversions of C_3H_6 and CO over Fe_2O_3/TiO_2 as a function of the reaction temperature in the absence and presence of SO_2.

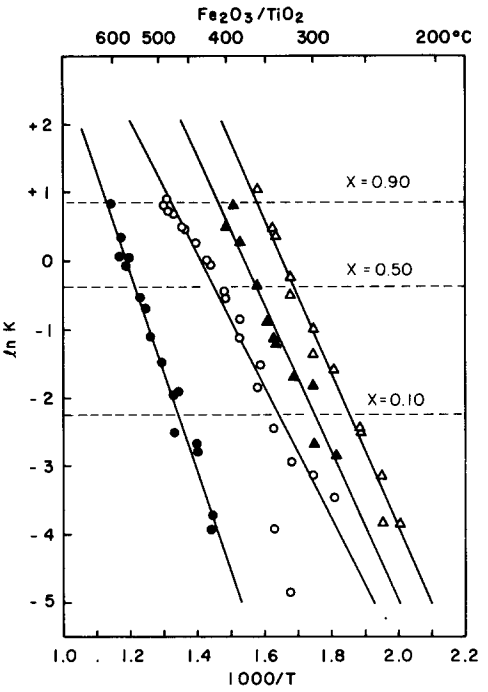

FIG. 4. Arrhenius plots of $\ln[-\ln(1-x)]$ versus $1000/T$, with x the degree of conversion and T the absolute temperature, for C_3H_6 and CO over Fe_2O_3/TiO_2. Feed composition: (△) C_3H_6; (○) CO; (▲) C_3H_6 + SO_2; (●) CO + SO_2.

showed that the first-order approximation was slightly superior, although the differences were small; this approximation was therefore used for all catalysts. Figures 5 and 6 present the plots of $\ln[-\ln(1-x)]$ vs $1000/T_x$ for Fe_2O_3 and Fe_2O_3/Al_2O_3 in the presence and absence of SO_2 in the feed.

The results for binary oxides, such as $FePO_4$, $FeSbO_4$, and $Fe_2(MoO_4)_3$, are markedly different, as shown by Figs. 7 and 8. Their rates of oxidation were much smaller, even in the absence of SO_2; they were more like those of Fe_2O_3 in the presence of SO_2 with rates of CO oxidation particularly low and hardly decreased by SO_2 addition. These catalysts were actually resistant to SO_2 poisoning, but at the cost of too drastic a decrease in activity to be interesting for the purpose of exhaust purification. In all binary catalysts there was a close agreement between CO converted and

TABLE 5

Summary of Experimental Results

Catalyst[a]	Feed component	T (K)[c]			Arrhenius parameters			
		10%	50%	90%	$-E$ (kcal/mole)	ln A'	R^d	n^e
Fe_2O_3	CO (<625 K)	600	(640)	(670)	26.4	19.9	0.965	8
	(>625 K)	(585)	671	735	16.1	11.7	0.988	13
	C_3H_6	570	630	670	27.4	21.7	0.987	15
"Up"	CO (+SO_2)[b]	750	826	880	39.5	23.4	0.996	7
"Up"	C_3H_6 (+SO_2)[b]	667	704	735	38.9	28.3	0.987	6
Fe_2O_3/TiO_2	CO	606	685	752	19.4	13.7	0.988	21
	C_3H_6	538	592	633	22.5	18.6	0.988	12
	CO (+SO_2)[b]	741	820	877	29.6	17.7	0.995	17
	C_3H_6 (+SO_2)[b]	571	633	680	22.5	17.4	0.971	11
Fe_2O_3/Al_2O_3	CO	535	600	650	20.0	16.4	0.970	22
	C_3H_6	515	565	608	22.6	19.7	0.978	13
"Up"	CO (+SO_2)[b]	658	719	(769)	26.9	18.4	—	4
"Down"	id	719	806	878	26.9	16.7	0.987	20
"Up"	C_3H_6 (+SO_2)[b]	549	600	(650)	25.7	20.7	0.997	5
"Down"	id	600	648	(685)	30.3	23.0	1.000	3
$FeSbO_4$	CO	⩾800	—	—	10.7	4.0	0.800	18
"Up"	C_3H_6	615	746	—	7.8	4.9	0.955	12
"Down"	C_3H_6	707	800	—	18.0	10.6	0.996	9
$FePO_4$	CO	⩾800			16.2	8.0	0.798	7
	C_3H_6	587	(800)	—	12.0	7.2	0.987	21
$Fe_2(MoO_4)_3$	CO	Not active						
	C_3H_6	718	>800		19.7	11.5	0.972	8

[a] Catalyst. "Up" signifies data points obtained only at rising temperature, "down" only at decreasing temperature.

[b] Feed component. "+SO_2," 40 ppm SO_2 also present.

[c] T (K)/y%, temperature (K) for y% conversion. If underlined, directly determined; if between brackets, extrapolated.

[d] R, correlation coefficient.

[e] n, number of data points.

CO_2 formed, showing that the oxidation of propene occurred without formation of CO_2. It is indeed well known that over these catalysts, propene is mainly converted to acrolein.

On the other hand, the properties of Fe_2O_3 supported on TiO_2 or Al_2O_3 were qualitatively similar to those of pure Fe_2O_3. The oxidation of propene in the absence of SO_2 started between 515 and 575 K depending on the catalyst. Temperatures needed for 90% conversion ranged between 610 and 670 K. Carbon monoxide oxidation started at a temperature slightly higher (20 K) than those for propene, but the 90% conversion temperatures for CO were much higher than those for propene, around 710 K. The average E' factor for the three catalysts was 19 kcal for CO oxidation and 24 kcal for propene oxidation.

Addition of SO_2 to the feed always produced a shift of the x–T scans to higher temperatures (Fig. 3), with the shift greater for CO oxidation. Defining T_y as the temperature needed to achieve y% conversion, we found T_{10} (SO_2 free)/T_{10} (with SO_2) to be

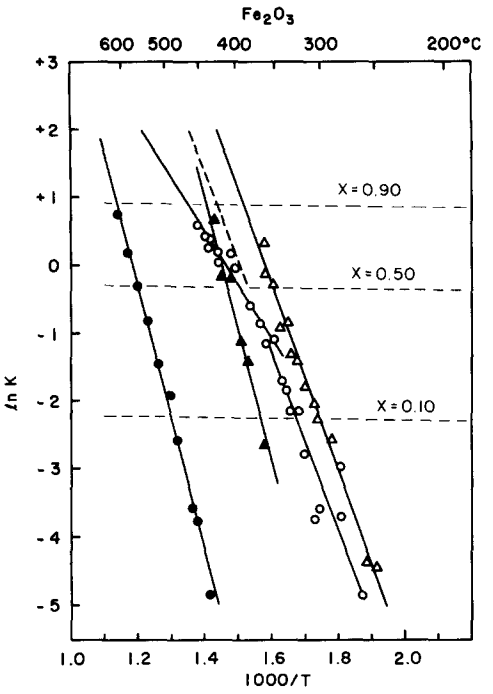

FIG. 5. Arrhenius plots for Fe_2O_3 as in Fig. 3. Feed composition: (△) C_3H_6; (○) CO; (▲) C_3H_6 + SO_2; (●) CO + SO_2.

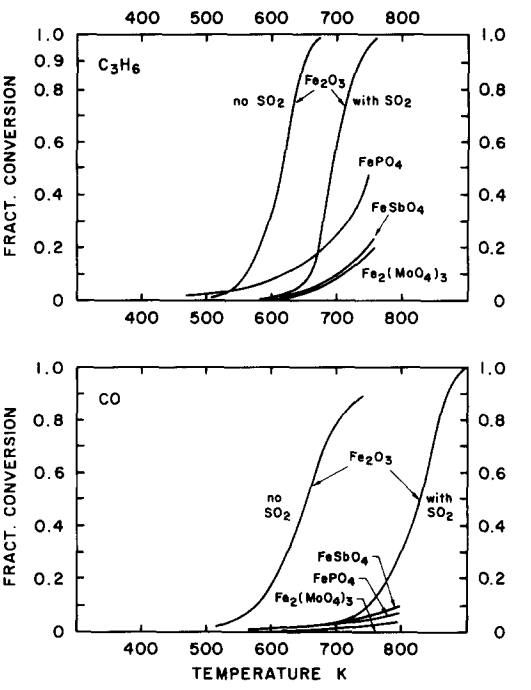

FIG. 7. Comparison of conversions of C_3H_6 over Fe_2O_3 and binary oxide in the presence of SO_2.

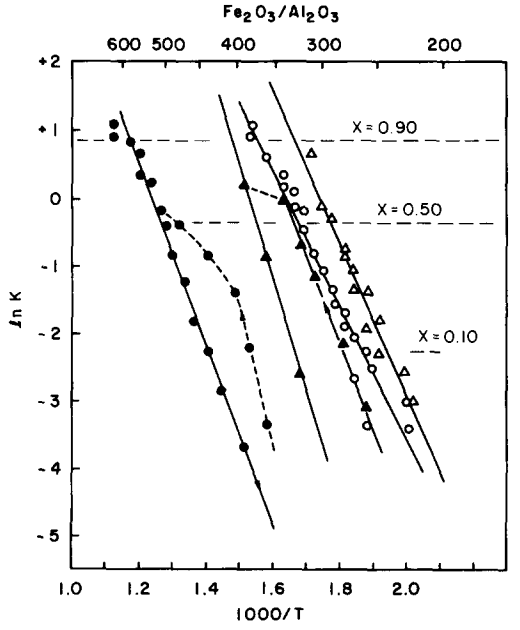

FIG. 6. Arrhenius plots for Fe_2O_3/Al_2O_3 as in Fig. 3. Feed composition: (△) C_3H_6; (○) CO; (▲) C_3H_6 + SO_2; (●) CO + SO_2.

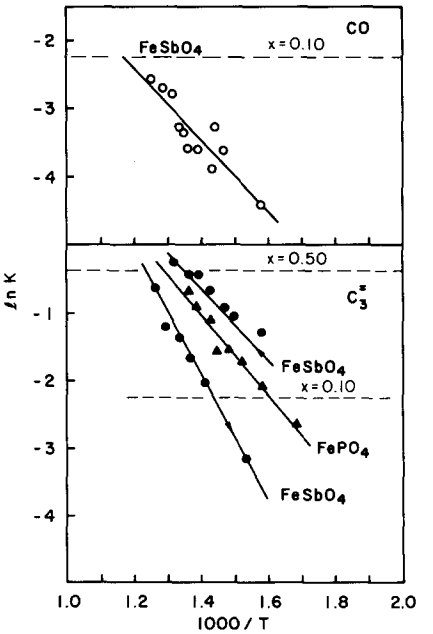

FIG. 8. Arrhenius plots of C_3H_6 and CO as in Fig. 3 but over $FeSbO_4$ and $FePO_4$. Feed composition: (○) CO; (●) CO + SO_2; (▲) C_3H_6 + SO_2.

0.79 for CO and 0.89 for C_3H_6 oxidation on Fe_2O_3 alone or supported. The average E' values in the presence of SO_2 were 29 kcal for CO oxidation; they varied from 23 to 45 kcal for propene oxidation. It is noteworthy that the T_{10} values for the alumina-supported sample were lower than those for pure Fe_2O_3 and for TiO_2-supported catalysts, in both the presence and the absence of SO_2. This indicates that Fe_2O_3 was more finely dispersed on the higher-surface-area alumina support.

The data with Fe_2O_3/Al_2O_3 also exhibited a hysteresis effect; i.e., conversions at increasing temperature ("up") and subsequently decreasing temperatures ("down") did not coincide. This seems typically connected with the change in the bulk structure of the Fe_2O_3 component mentioned above. A similar hysteresis effect was observed with $FeSbO_4$ (Fig. 8), where the "upward" mode gave ln A' and E' values of 4.9 and −7.8, while the "downward" mode gave 10 and −18. We speculate that this change occurred because of a redistribution of surfacial antimony to the bulk during the warm-up period to 500°C although XPS evidence for this was inconclusive.

In all three Fe_2O_3 catalysts, when SO_2 was present in the feed, CO oxidation started only at temperatures where propene oxidation was already complete. In this case, a detailed inspection of the analytical results allowed an estimate to be made of whether propene oxidation was partial or complete from the difference between the amounts of CO converted and CO_2 formed. In the absence of SO_2, it proved impossible to obtain reliable results because the ratio of CO to propene in the feed was high (100) and the oxidation temperature ranges overlapped.

Results previously obtained for butene oxidation over orthorhombic Fe_2O_3 indicate that considerable amounts of butadiene (a partial oxidation product) are produced in the range 650–750 K, accounting for half of the olefin consumed to temperatures up to at least 790 K (*9*).

In the cases presented here, propene was partially oxidized (no CO_2 was formed) when SO_2 was also present in the feed. In an isothermal run at 660 K, CO conversion dropped to almost zero when SO_2 was introduced in the feed, while propene conversion maintained its 30% conversion level, indicating that it occurred without C–C bond breaking. Similar results were obtained with $FeSbO_4$.

The analysis of all data also indicated that CO and H_2 were oxidized simultaneously. This was determined from a comparison of the amount of CO + C_3H_6 oxidized with the amount of oxygen consumed.

The plots for E vs ln A' for propene and CO oxidation can be fit by the linear relationship

$$-E = P + Q \ln A', \qquad (2)$$

indicating that these reactions follow a compensation law (Fig. 9). Line I includes all points for the three Fe_2O_3 catalysts, for

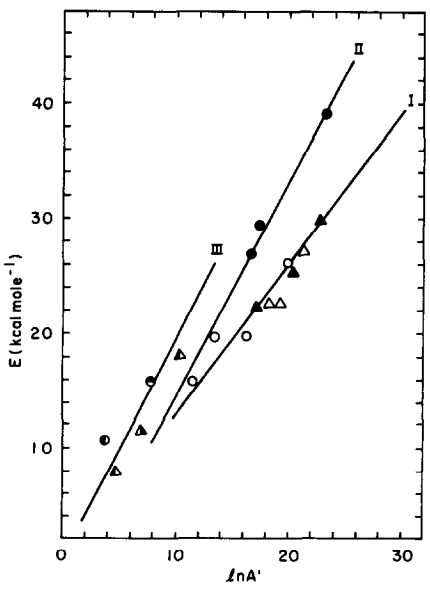

FIG. 9. Compensation law ($-E$ vs ln A') for oxidation reactions over the iron containing catalysts. Open symbols, reactions without SO_2; filled symbols, reactions with SO_2; half-filled, binary catalysts. Reactions of CO given by circles, those of C_3H_6 by triangles.

CO oxidation in the absence of SO_2 in the feed, and for propene oxidation with and without SO_2 in the feed. The P and Q parameters are -7.29 and $-1{,}326$ with $R = 0.97$. Line II covers the same set of catalyst for CO oxidation in the presence of SO_2. Its parameters are: $P = 7.98$, $Q = -2.04$, $R = 0.96$. Lines I and II intersect at $E = 10.5$, $\ln A' = 8.5$. Line III includes all experiments with CO and propene done over binary oxides and runs almost parallel to line I at a distance $\Delta \ln A' = -4$. Its parameters are $P = -2.96$, $Q = -1.44$, and $R = 0.93$.

Figure 10 also includes data for separate butene and CO oxidation over $FeSbO_4$ impregnated with either Fe(III) or Sb(III) (*9*). The plot shows a linear compensation law relation with $P = -2.96$, $Q = -1.24$, and $R = 0.997$. (Note that the line runs parallel to line I of Fig. 9, but it is shifted to lower $\ln A'$ values.)

DISCUSSION

The main item in the forthcoming discussion is the different sensitivity to SO_2 poisoning of the C_3H_6 oxidation on the one hand and that of CO and H_2 on the other. In trying to explain this difference, we start from the following assumptions.

(1) All surface sites on a pure Fe oxide surface are similar, and the oxidation of C_3H_6, CO, H_2, and SO_2 occurs on the same sites.

(2) If iron oxide sites become partially covered by an inactive species, the average number of contiguous oxygen sites, the ensemble, becomes smaller and the number of sequential reactions involving those sites is restricted. Hence, oxidation may become partial instead of complete as on a "free" surface (*12*). (See Straguzzi *et al.* (11) for further proof that the ensemble theory is useful to explain selectivities in oxidation reactions.)

Inhibition by SO_2 is generally accepted (*1–5*) to involve formation of sulfate groups on the surface oxygens; oxidation of other feed components then can occur only at temperatures high enough to cause decomposition of these surface sulfate groups. The decomposition enthalpies of surface sulfate groups will be smaller than those of bulk sulfates, since only a fraction of their oxygens are bonded to other cations, this fraction being in the order of one-half. Another compound that can give rise to surface blocking is CO which may form carbonate groups. The enthalpies, and thus free energies, of formation of transition metal carbonates are on the average 40 kcal/mole smaller than those of the sulfates (*13*); desorption of CO_2 from a carbonate-covered surface will hence take place at considerably lower temperatures than that of SO_3 from a sulfate-covered surface. The data indicate that CO_2 does not play a significant role as an inhibitor in our reactions.

Strong inhibition of catalytic olefin oxidation by partial oxidation products, such as acrolein from propene or butadiene from butene, is frequently mentioned in the literature; these two examples are usually reported as very similar (*10*). The results of Matsuura (*14–16*) lead us to use the following simplified surface model to explain our data.

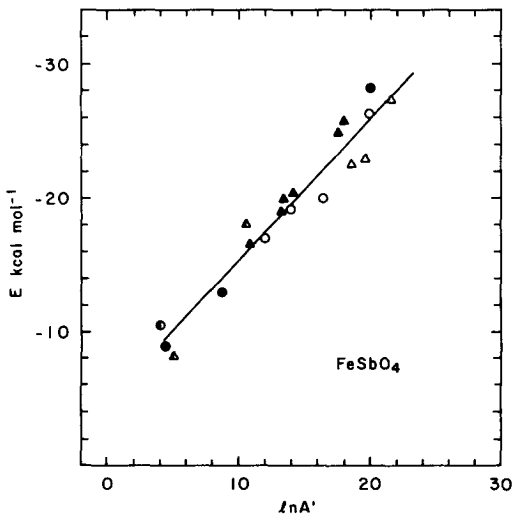

FIG. 10. The compensation law as valid for the data of Straguzzi *et al.* (*11*) with butene or CO as the feed and $FeSbO_4$ catalysts with varying ratios of Sb/Fe at the surface (filled symbols). Note that this line runs approximately parallel to line I (Fig. 8).

Propylene (or butadiene) adsorption on an Fe_2O_3 surface is irreversible up to at least 250°C with formation of a closely packed (C) layer that consists mainly of carbon with some hydrogen bonded to a sublayer, named the "O layer," that was originally the surface of the solid oxide. If the double layer is exposed to inert gas at high temperatures, it will decompose locally into CO_2 and H_2, the oxygen being derived from the catalyst by a Mars–van Krevelen mechanism. Simultaneously, "holes" are formed in the carbonaceous (C) layer and "vacancies" are formed in the adjacent oxide (O) layer. In a more advanced state of decomposition, there will be agglomerates of holes and vacancies. Their number and size will increase when the temperature becomes higher. When heated in the presence of O_2, the O vacancies will be refilled with O^2 cations, the combination of O^2 ions and holes being obviously identical to what was earlier defined as an ensemble. When an olefin is also present, it will react with the oxygens in the ensemble, and the way it interacts is defined by the size of the ensemble; small ensembles will give acrolein and large ensembles will produce multiple-bonded species that will lead to a repair of the C layer and, therefore, in the long run to a formation of CO_2 and H_2O. At relatively low temperatures, the most frequent ensembles will be small and they will produce only partial oxidation products. Thus, on heating from lower to higher temperatures in the presence of olefin and oxygen, there is first the formation of the C layer covering the entire Fe_2O_3 surface; then, at higher temperatures, formation of intermediate products, such as acrolein; and at more elevated temperatures, the reaction products will be CO_2 and H_2O, as observed earlier (*11, 14–16*). This set of events occurs in the range 500 to 650 K and is represented by the Arrhenius plots for the propene oxidation in the Figs. 3–5 for the oxidation of propene. Straguzzi *et al.* have reported (*11*) that in the presence of butene or butadiene CO oxidation did not occur. Similarly, we found that in mixture with propene, oxidation of CO and H_2 always came after propene had been largely converted. On a "clean" surface, H_2 reacts together with CO and they react after propene. Apparently, the products of propene oxidation, particularly the formation of the C layer, are the main agents for poisoning at lower temperatures.

To fit inhibition by oxidized SO_2 into our model, we assume that the oxidation of SO_2 to SO_3 is also inhibited by the C layer and can take place only after the extent of the C layer and/or of acrolein inhibition was substantially reduced, i.e., above 600 K (see Fig. 11).

The situation above 600 K is complex because inhibition by products of propene oxidation is not extensive enough to prevent the oxidation of SO_2, and as a consequence, poisoning by SO_3. Between 600 and 650 K there is a mixed regime with both inhibitors operating. There is still no CO oxidation: the expected rate increases because the diminished inhibition by propene products is eliminated by the newly created SO_3 adsorption. Above about 650 K, the

Surface	C layer	Mixed	SO_4^{2-} layer	Empty
Propene	No reaction →	C_3H_4O	C_3H_4O	CO_2
CO	No reaction	No reaction	No reaction	CO_2
SO_2	No reaction	Start	$\rightarrow SO_4^{2-}$	$\rightarrow SO_3$
		600 K	650 K	730 K

FIG. 11. Model for the reactions and the state of the Fe_2O_3 as a function of the temperature in the presence of SO_2. Temperatures are somewhat variable with the catalyst.

surface is presumably covered by a sulfate layer that entirely inhibits CO oxidation.

It is not clear what happens to propene from our data: gc analysis shows that it disappears because of some reaction. We propose that the oxidation is partial. This conclusion is based on the results of the run at the constant temperature of 660 K where propene oxidation occurred without production of CO_2. Moreover, in temperature scans, it is noticeable that the ratio of "CO_2 formed" to "CO converted" is still near to 1 and only begins to rise when SO_3 starts to desorb. The sulfate groups thus have an influence similar to that of antimony oxide in the binary oxides; they restrict the ensemble size and make the oxidation selective. The discrepancy between the sensitivities of C_3H_6 and CO to the inhibition by SO_3 is then only deceptive; the complete oxidation was indeed inhibited, just as the CO oxidation, but partial oxidation continued. This might be another reason to reject Fe oxide catalysts for exhaust purposes: catalysts that up to 700 K emit acrolein to the environment do not seem particularly attractive.

We generalize these observations to conclude that every inhibitor, H_2O, CO_2, C_3H_4O, C layer, or SO_3, is created by oxidation of a precursor, H_2, CO, C_3H_6, or SO_2, and its oxidation can be inhibited by the product of another feed component. Thus, the reactivity of the reactant on a "clean" surface and the Gibbs free energy of the various products on the surface are both important.

Support for the concept of ensemble-size control of oxidation selectivity also comes from oxidation results with surface-doped $FeSbO_4$ catalysts. On $FeSbO_4$ with extra Sb_2O_4 on its surface, nonselective oxidation only takes place above 1300 K, where Sb_2O_4 volatilizes from the surface. Only when the surface of $FeSbO_4$ is impregnated with extra Fe^{3+} so that the Sb/Fe ratio becomes lower than 2, does extensive combustion become observable at lower temperatures (*9, 11*).

Our interpretation of the data is also supported by a compensation law analysis. The two sets of experiments presented in Figs. 9 and 10 show E versus ln A lines, of which line I in Fig. 9 showed almost the same slope as the single line in Fig. 10. Both lines had to do with the oxidation of olefins and presumably with the desorption of a product, acrolein in Fig. 9 and butadiene in Fig. 10. Moreover, the Fig. 10 experiments incorporate the runs in which the ensemble size was deliberately changed by impregnation with Fe or Sb salts. This led to changes in activity and selectivity that were correlated; larger Fe ensembles were more active but less selective, both effects being incorporated in the results of the figure. The similarity with the line I results in Fig. 9 leads us to postulate that the combinations of phenomena occurring in the two cases are closely similar.

The change from organic-product kinetics to "clean surface" kinetics can be seen in the break in the ln k vs $1/T$ plot for the oxidation of CO on Fe_2O_3 (Fig. 5), where the Arrhenius parameters ($-E$, ln A) fall from (-26,20) to (-16,12) at 625 K. Acrolein adsorption and/or the C layer is assumed to disappear at this temperature; the surface would thus be "clean" above 625 K. The fact that the plot of ln k–$1/T$ for CO oxidation below 625 K runs approximately parallel to that of that for C_3H_6 oxidation (with parameters (-27, 22)) supports the hypothesis that below 625 K the surface is covered by a partial oxidation product of propene.

Let us consider the similarity in the compensation law plots of Figs. 9 and 10 in more detail. If the rate of a heterogeneous reaction that is inhibited by a strongly adsorbed reactant or product or by a catalyst poison (such as SO_3) is plotted according to Arrhenius, the line is not straight but is curved, as is well known. For instance, consider the reaction $A \rightarrow \underline{A} \rightarrow \underline{A}^{\ddagger} \rightarrow \underline{P} \rightarrow P$, where A is the reactant, $\underline{A}$ the adsorbed molecule, $\underline{A}^{\ddagger}$ the adsorbed transition state, $\underline{P}$ the adsorbed product, and P the desorbed product. According to the "absolute rate" theory, activation energy and entropy are

defined by the difference in enthalpy and entropy between the molecule in the gas phase and on a site at the surface. If the temperature is high enough for the surface to be empty, let the activation enthalpy be $\Delta H^{\ddagger}$ and the entropy by $\Delta S^{\ddagger}$. At a temperature low enough to have the surface almost completely covered by A, hence $\theta_a \sim 1$, an adsorbed molecule $\underline{A}$ should be excited to the transition state for which it needs an enthalpy, equal to $\Delta H^{\ddagger} + \Delta H_{ads}(A)$, the adsorption enthalpy. To evaluate the activation entropy, it is sufficient to consider that the replacement of $\underline{A}$ by $\underline{A}^{\ddagger}$ does not involve changes in translational entropy so $-\Delta S^{\ddagger} + \Delta S_{ads}(A) \simeq 0$. The description of the process defining the activated state is accordingly different and dependent on the temperature although the situation is basically the same: at a low temperature, activation energy and preexponential may both be high, while at a high temperature they are both low. Similar corrections must be introduced when the surface is covered by the adsorbed products at low temperature. The activation energy is then $\Delta H^{\ddagger} + \Delta H_{ads}(P)$ and the entropy $-\Delta S^{\ddagger} + \Delta S_{ads}(P)$. Since enthalpies of adsorption are usually greater for butadiene and acrolein than for the olefins, product adsorption will be more common than that of the reactants. More often than not the temperature ranges over which activities are measured will be smaller than those between the two extremes discussed so far and the representative points for various sets of measurement will be scattered between these two in the E–ln A plane giving the impression of a line that should not necessarily be straight, but might be approximately so.

CONCLUSIONS

The results of this study are consistent with the following interpretation.

(1) The kinetics of the combined oxidation of C_3H_6, CO, and H_2 over Fe oxide catalysts are determined by the presence of surface layers on top of the oxide surface. Oxidation inhibitors, such as H_2O, CO_2, C_3H_4O, C layer, or SO_3, are created by oxidation of a precursor, H_2, CO, C_3H_6, or SO_2, whose oxidation can be inhibited by the product of another feed component. Thus, the reactivity of the reactant on a "clean" surface and the Gibbs free energy of the various products on the surface are both important.

(2) For Fe_2O_3 alone, or supported on TiO_2 or Al_2O_3, the surface layer in the absence of SO_2 consists of a carbonaceous material ("C layer") that is already formed at room temperature but which decomposes between 570 and 625 K. If SO_2 is present, there is another layer, formed above 625 K, that has the surface covered with sulfate groups; these decompose again above 800 K. Binary Fe oxides, such as $FeSbO_4$, have the surface covered by layers of Sb oxide that are stable up to temperatures as high as 1200 K; below that temperature they can be changed only by impregnation with the component materials.

(3) The C layer and the sulfate layer contain defects, holes, or oxygen ensembles that grow in number and size with increasing temperature.

(4) Oxidation of propene on small ensembles is partial and produces acrolein that can act as an inhibitor; it can, for instance, inhibit the oxidation of SO_2 to SO_3. Once SO_3 is formed, it can adsorb as a sulfate group and inhibit the oxidation of propene to CO_2 and H_2O. The two inhibitor systems, therefore, seem to counteract each other.

(5) The presence of the minor compounds, propene and SO_2, determines the temperature at which the major compounds, CO and H_2, are oxidized; propene alone fixes the lower limit at 625 K, propene + SO_2 at about 800 K.

ACKNOWLEDGMENTS

We thank Dr. Paden Dismore, Dr. Julia Onuferko, and Dr. Brian Strohmeier for their assistance in XRD and XPS measurements and their interpretation of the data. Rashev Joshi is thanked for his help in reactor construction, Pankaj Mehta for the Pt/Al_2O_3 data, and Jack Hollobaugh for technical help and advice. We especially want to acknowledge the generous financial

support from General Motors and the interest shown in our work by Dr. John Larson.

REFERENCES

1. Kummer, J. T., *Adv. Chem. Ser.* **143,** 178 (1975).
2. Hegedus, L. L., and McCabe, R. M. W., *Catal. Rev.* **23,** 377 (1981).
3. Farrauto, R. T., and Wedding, B., *J. Catal.* **33,** 249 (1973).
4. Yao, Y-F. Y., *J. Catal.* **39,** 104 (1975).
5. Lowell, P. S., Schwitzgebel, K., Parsons, T. B., and Sladek, K. J., *Ind. Eng. Chem. Process Des. Dev.* **10,** 384 (1971).
6. JCPDS International Center for Diffraction Data, X-Ray Diffraction Powder Patterns (1983).
7. JCPDS International Center for Diffraction Data, X-Ray Diffraction Powder Patterns, Card 24 18 (1983).
8. Walker, J. S., MS. thesis, Chem. Eng. Dept., University of Delaware, 1984.
9. Straguzzi, G. I., Bischoff, K., Koch, T., and Schuit, G. C. A., *J. Catal.* **103,** 357 (1987).
10. Burban, P. M., Ph.D. thesis, Chem. Eng. Dept., University of Delaware, 1984.
11. Straguzzi, G. I., Bischoff, K. B., Koch, T. A., and Schuit, G. C. A., *Appl. Catal.* **25,** 257 (1986); *J. Catal.* **104,** 47 (1987).
12. Callahan, J. L., and Grasselli, R. K., *AIChE J.* **9,** 755 (1963).
13. "Handbook of Chemistry and Physics" (R. C. Weast, Ed.), 63rd ed. The Chemical Rubber Co., 1982–1983.
14. Matsuura, I., *J. Catal.* **33,** 420 (1973).
15. Matsuura, I., and Schuit, G. C. A., *J. Catal.* **20,** 19 (1971).
16. Matsuura, "Proceedings, 6th International Congress on Catalysis, London, 1976" (G. C. Bond, P. B. Wells, and F. C. Tomkins, Eds.), Vol. 2, p. 819. The Chemical Society, London, 1976.